Journal of Applied Polymer Science

Densifying and strengthening of electrospun polyacrylonitrile-based nanofibers by uniaxial two-step stretching

Je Sung Youm,[1,2] Ji Hoon Kim,[1,2] Chang Hyo Kim,[1,2] Jeong Cheol Kim,[3] Yoong Ahm Kim,[1,2] Kap Seung Yang[1,2]

[1]Alan G. MacDiarmid Energy Research Institute, School of Polymer Science and Engineering, Chonnam National University, 77 Yongbong-Ro, Buk-Gu, Gwangju, 500-757, Republic of Korea

[2]Department of Polymer Engineering, Graduate School, Chonnam National University, 77 Yongbong-Ro, Buk-Gu, Gwangju, 500-757, Republic of Korea

[3]Korea Institute of Industrial Technology, 6 Cheomdangwagiro 208 Beongil, Buk-Gu Gwangju, 500-480, Republic of Korea

Correspondence to: Y.A. Kim (E-mail: yak@jnu.ac.kr) and K. S. Yang (E-mail: ksyang@jnu.ac.kr)

ABSTRACT: The effects of alignment of polyacrylonitrile (PAN) nanofibers and a two-step drawing process on the mechanical properties of the fibers were evaluated in the current study. The alignment was achieved using a high-speed collector in electrospinning synthesis of the nanofibers. Under optimal two-step drawing conditions (e.g., hot-water and hot-air stretching), the PAN nanofiber felts exhibited large improvements in both alignment and molecular chain-orientation. Large increase in crystallinity, crystallite size, and molecular chain orientation were observed with increasing draw ratio. Optimally, stretched PAN-based nanofibers exhibited 5.3 times higher tensile strength and 6.7 times higher tensile modulus than those of the pristine one. In addition, bulk density of the drawn PAN nanofibers increased from 0.19 to 0.33 g/cm^3. Our results show that fully extended and oriented polymer chains are critical in achieving the highest mechanical properties of the electrospun PAN nanofibers. © 2016 Wiley Periodicals, Inc. J. Appl. Polym. Sci. **2016**, *133*, 43945.

KEYWORDS: electrospinning; mechanical properties; nanostructured polymers

Received 10 December 2015; accepted 19 May 2016
DOI: 10.1002/app.43945

INTRODUCTION

In recent years, nano-sized fibers have aroused a large interest due to their distinctive mechanical, physical, and chemical properties, which are useful in different applications. Nanofibers are industrially important[1] and have found a wide variety of applications due to their high specific surface area, flexibility, and large aspect ratio that originated from their nano-sized diameter.[2] Polyacrylonitrile (PAN) nanofibers, for instance, have recently become popular as a precursor to carbon nanofibers, which can be used as the electrode materials in energy storage devices, bone tissue scaffold, heat-management materials, composite reinforcement, high-temperature catalysis, and membrane-based separation.[3–5]

Yao *et al.*[6] introduced a few novel techniques for the production of nanofibers, such as nozzle-less electrospinning with a rotating head, multi-nozzle electrospinning with a twin-screw extrusion, and rotary jet-spinning. The electrospinning system is a simple and efficient technique for the fabrication of nanofibers with diameter ranging from nano- to micro-scale.[7–10] Electrospinning is a highly versatile method as it is applicable virtually to every soluble or fusible polymer.[11] Nanofibers can be produced from polymer solutions using an electrospinning setup, which is composed of three main parts, viz. a syringe with a needle, a high voltage power supply, and a collector. Electrospinning is a potential method to produce uniform and continuous nanofibers from hundreds of polymers at a relatively low cost. Although the method is simple, formation of the fibers and their deposition on a target are influenced by many parameters.[10] So the electrospinning parameters related to materials, spinning solutions (such as concentration, electrical conductivity, and surface tension), electrospinning process (feed rate, electrode separation and geometry, and applied voltage), temperature, and relative humidity need to be controlled and optimized judiciously to achieve the highest outcome.[11] The fiber diameter increases as molecular weight or the solution concentration of a polymer increase. Interfiber spacing also increase and there is gradual shift from circular to flat fibers as the solution concentration increases.[12] However, if the concentration of the solutions is too high, the viscosity increases and it

Additional Supporting Information may be found in the online version of this article.

becomes difficult to produce thin fibers. However, too dilute solutions will result in the jet breaking into droplets.[13] The surface tension and viscoelasticity of the polymer solution are the key parameters that influence the formation of beaded fibers. An increase in the net charge density on the droplet favors the formation of small diameter fibers, whereas a decrease in the surface tension coefficient of the solvent favors the formation of large diameter fibers.[14]

Electrospun nanofibers typically display tensile strengths below 300 MPa and Young's modulus below 3 GPa.[6,15–17] Previously reported work on the mechanical properties of PAN nanofibers in relation with alignment and drawing is summarized in Supporting Information Table S1. It is regarded that poor mechanical properties of PAN-based nanofibers are mainly due to random alignment of electrospun nanofibers, low molecular chain orientation, and presence of surface defects on the fibers with large fiber diameters. Therefore, the basic essentials to achieve high-performance nanofibers comprise uniaxial alignment, molecular chain orientation, and reduction in the amount of defects on the surface of the nanofibers through drawing approach.

The electrospun nanofibers are usually deposited randomly on the target due to unstable motions, such as whipping, bending, and buckling. The electrospinning-jet instabilities hinder aligning of the nanofibers severely.[18] To enhance the ultimate mechanical properties of PAN nanofibers, the spun fibers have to be deposited with uniaxial alignment. Since a decrease in the instabilities could help the nanofibers in aligning, various methods have been proposed to control the fiber alignment. For example, auxiliary electrode (aluminum grid behind the target),[8] rotating auxiliary electrode (aluminum plates between nozzle and collector),[10] back metal electrodes,[17] back electrode plate (guard plate) behind the electrospinning emitter,[18] a rotating drum collector,[19–21] additional centrifugal field,[22] collecting in flowing water bath,[23] magnetic field-assisted,[24] conductive silicon strips separated by void gap,[25] rotating metal disk collector,[26] and U-shaped metal device[27] were adopted for fabricating uniaxially aligned nanofibers.

The mechanical properties are known to substantially improve with an increase in the molecular chain orientation and decrease in the fiber diameter. High degrees of orientation can be achieved if the distance between the electrodes is reduced to the centimeter or millimeter range, and if either the spinning electrode or the counter electrode has the shape of a fine tip.[11] The large diameter and defects are the major factors to weaken the tensile strength of PAN-based nanofibers.[6,21,27,28] Drawing of the spun fibers above T_g (72–150 °C)[17] and below cyclization temperature is greatly effective in orienting the molecular chains along the direction of drawing. At this orientation, the molecular dipole interactions between the nitrile groups of PAN decreases and the physical properties improves, resulting in removal of potential weak points in the PAN nanofibers.[29,30]

Recent observations show that both the molecular orientation and the degree of crystallinity of the electrospun fibers are high due to huge elongation during spinning.[3] The degree of molecular orientation and crystallinity of the electrospun fibers, however, are limited and insufficient for realizing maximal performance of the PAN nanofibers. So, drawing after electrospinning can be a critical process to achieve a high level of molecular chain orientation, which in turn could impart improved mechanical properties to the PAN nanofibers.

In the present study, novel methods have been developed to synthesize PAN-based nanofibers with improved mechanical properties. To produce highly aligned PAN nanofibers during electrospinning, we first optimized the key spinning parameters as well as the electrospinning setup, which was composed of deflector plates and high-speed rotating target drum. In addition, the drawing process allowed us to obtain highly aligned as-spun nanofibers, thereby resulting in the formation of highly oriented molecular chains, increased crystallinity and large crystallite size in the nanofibers. A decrease in the amount of defects formed in the drawn nanofibers was also expected since the drawing process should impart more perfection to the morphological structure.[17,31] Investigations and characterizations of the aligning and drawing effects on the PAN nano-fibers are presented in this report.

EXPERIMENTAL

Materials and Electrospinning Solution

Polyacrylonitrile (PAN, M_w 150,000 g/mol, Pfaltz & Bauer Chemical CO. USA) was used as the polymer. Dimethyl sulfoxide (DMSO) from Sigma-Aldrich was used as the solvent without further purification. The solution for electrospinning was prepared by dissolving 12 wt % of PAN in DMSO at 80 °C with stirring for 4 h. For a direct comparison, the mechanical properties of commercial PAN fibers (12 K PAN fibers produced by Bluestar Fibers Company Limited) were evaluated.

Electrospinning

Electrospinning setup was designed for high-speed fiber-collection and utilizing deflector plates to obtain highly aligned electrospun PAN-based nanofiber felts. The electrospinning set-up consisted of a syringe containing the spinning solution, two high voltage power suppliers, one of which was for the nozzle and another was for the deflector plates, and a rotating speed-adjustable drum collector. The spinning capillary nozzle of a metallic needle was attached at the tip of the syringe, which had an inner diameter of 0.41 mm. The syringe with the spinning capillary was placed horizontally to the collector. The rotating speed of the collecting drum could be varied up to 2,000 m/min and was grounded. Two deflector plates were added for further alignment of the fibers by restraining the bending and buckling instabilities during the electrospinning process. Rectangular aluminum plates were used as the deflector plates with thickness of 5 mm. The solution feeding rate was 1.0 mL/h at 17–23 kV on the spinning nozzle and 8–12 kV at deflector plates. The rotation speed of the collecting drum was adjustable in the range 500–2,000 m/min, and was fixed to 2,000 m/min to obtain samples for study. The spun fibers were collected for 7–8 h without breaking. Electrospinning was carried out at ambient temperature (20–25 °C) and humidity (30–50%). The electrospinning setup and the aligned electrospun PAN nanofibers are shown in Supporting Information Figure S1.

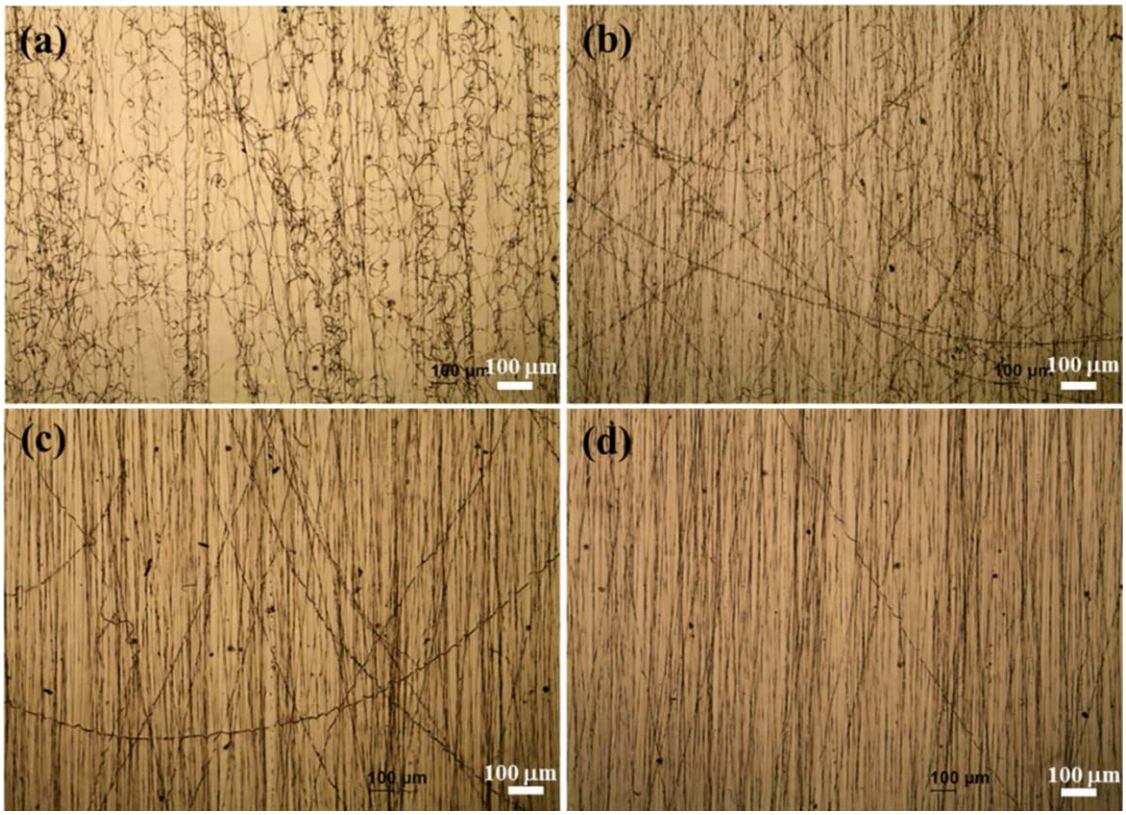

Figure 1. Optical microscopy photographs of electrospun PAN nanofiber felts for 3 min winding at drum speed of (a) 500 m/min, (b) 1,000 m/min, (c) 1,500 m/min, and (d) 2,000 m/min. [Color figure can be viewed in the online issue, which is available at wileyonlinelibrary.com.]

Drawing

The aligned electrospun PAN nanofibers were drawn in one direction along the fiber axis for improved uniaxial orientation of the molecular chains. Drawing was conducted in two steps. In the first step, samples were drawn uniaxially in water in the temperature range of 90–95 °C. In the second step, they were further drawn uniaxially under dry hot air at a temperature of 160 °C. This temperature was selected after a pretest from 80 to 180 °C at an interval of 20 °C. The temperature range of 80 to 180 °C is actually the range of glass transition (T_g) and cyclization temperature of PAN. The fiber web was placed horizontally and both its ends were held tightly on metal grippers. The specimens were kept in the drawing chamber for about 10 min at the target temperature and drawn at the rate of 0.5 mm/s (Supporting Information Figure S2). The drawn samples were kept under tension by fixing them on the glass plate or hanging them up on the rack with a weight load under gravity for about 24 h to prevent any contraction.

Characterization and Evaluation

The surface morphology of PAN nanofibers sputter-coated with Pt was observed through a field-emission scanning electron microscope (FE-SEM). Polarized Fourier transform infrared spectroscopy (FT-IR) spectra were acquired using a Nicolet 50 FT-IR spectrometer equipped with a polarizer. The 2 Theta-Omega scan and azimuthal scan were carried out using X-ray diffractometer (X'pert APD, Philips) and high resolution X-ray diffractometer generated by long fine focus (LFF) Cu anode (3 kW). The 2 Theta-Omega and azimuthal scans were performed at a voltage of 40 kV and tube currents of 30 mA and 25 mA, respectively. Differential scanning calorimetric (DSC) experiments were carried out under dry nitrogen by using a Diamond DSC (Perkin-Elmer) at a heating rate of 10 °C/min. The second scanned DSC curve was obtained after quenching at a rate of 150 °C/min. The tensile properties of the nanofiber felts were measured by the Universal Testing Machine (Instron 5543, see in Supporting Information Figure S3) using a gauge length of 20 mm, where strain rate was 2 mm/s and load cell was 50 N.

RESULTS AND DISCUSSION

The rotating speed of the correcting drum was varied as 500, 1,000, 1,500, 2,000 m/min and the best alignment of the nanofibers was observed at 2,000 m/min (Figure 1). The jet speed was calculated as 1.26 m/min at the syringe tip. Furthermore, the jet stretch on the spin line was calculated as more than 1,580 times at 2,000 m/min with no consideration of splitting. The draw ratio we achieved in boiling water was about 2. Drawing in dry air was carried out to find out the temperature showing the highest draw ratio in the temperature range from 80 to 180 °C, at intervals of 20 °C. It was confirmed that the highest draw ratio can be achieved at the temperature of 160 °C which matched with the previously reported value.[32] The maximum draw ratio we achieved was about 3 on average by drawing in dry air (Supporting Information Figure S4 and Table 1). The two times drawn nanofiber in hot water (water as plasticizer, Supporting Information Figure S5) were stretched again in dry

Table I. Draw Ratios without Breaking Using One-Step and Two-Step Drawings

Drawing step	Drawing condition (Temp.)	Draw ratio			
1st step	In boiling water (90–95 °C)	X	X	2	2
2nd step	In hot dry air (160 °C)	X	3	2	2.5
Total draw ratio		1	3	4	5

air (Supporting Information Figure S6). The maximum draw ratio obtained was 5 because the samples drawn in the first step can be maximum drawn to about two times, as summarized in Table I. Since PAN has strong dipole force between the nitrile (–CN) groups, the interaction between the highly polar nitrile groups hinders the polymer chain to be drawn. Water acts as a plasticizer because the strong intermolecular interaction between the nitrile groups weakens in water at high temperature. It is expected that water molecules interact with the nitrile groups over 95 °C by decoupling nitrile–nitrile association and forming hydrogen-bonds instead with the nitrile groups.

The scanning electron microscopic (SEM) images [Figure 2(a–d)] show fiber surfaces of the aligned (1) as-electrospun PAN nanofibers, (2) stretched by three times, (3) four times, and (4) five times from the original length. The average diameters of the nanofibers were 744, 454, 321, and 302 nm for the as-electrospun sample, three, four, and five times stretched samples, respectively (see Supporting Information Table S2). The surface of the as-electrospun nanofibers was homogeneous, smooth, and do not have beads but the drawn samples showed shark skin surfaces along the fiber axis. The diameters of the nanofibers [Figure 2(e)] decreased with increasing draw ratio without any breakage of the individual fibers, expecting even higher stretching for more molecular orientation.

Polarized FT-IR analysis has been used as an effective approach to study the degree of molecular chain orientation in electrospun nanofibers.[19,33–36] FT-IR equipped with a polarizer was employed to analyze the molecular chain orientation in the PAN nanofiber felts depending on the draw ratio under parallel and perpendicular angles to the fiber axes. The molecular chain orientation can be characterized by the orientation function defined by the infrared dichroism. The infrared dichroism to determine the orientation function follows the eqs. (1–3).

$$D = \frac{A_{\parallel}}{A_{\perp}} \tag{1}$$

$$D_0 = 2\cot^2\alpha \tag{2}$$

$$f_{ch} = \frac{(D_0 + 2)(D - 1)}{(D_0 - 1)(D + 2)} \tag{3}$$

where f_{ch} is the degree of molecular chain orientation and α is the angle between the transition moment and the chain axis. D is the infrared dichroic ratio for the nitrile absorptions and defined as the ratio of $A_{\parallel}$ and $A_{\perp}$, which are the absorbance of the parallel and perpendicular spectra to the nanofiber drawing direction, respectively, and D_0 is the dichroic ratio of an ideally oriented polymer.[22,31,33] The characteristic absorption of nitrile-stretching (C≡N) vibration at ~2,244 cm^{-1} can be utilized to measure the orientation function of the molecular chains in the PAN nanofibers.[7,21,22,36] So, the degree of molecular chain orientation in PAN nanofibers can be evaluated by comparing the nitrile absorption peaks of the as-spun and drawn samples. The α for PAN was taken as 70, which is used for the evaluation of PAN molecular chain orientation.[22,33,37] The polarized FT-IR spectra of the as-electrospun and drawn nanofiber felts were normalized and compared [Figure 3(a)].[31] The peaks corresponded to the characteristic absorption of nitrile-stretching vibration at ~2,244 cm^{-1}. The molecular chain orientation of the as-electrospun nanofibers was improved by the drawing process, indicating that the drawn nanofibers were highly oriented. When the fiber axis was parallel to the incident beam at the polarization angle of 90, the C≡N absorption reached the maximum as a result of the resonance between the nitrile stretching and the electric field of the polarized incoming IR beam.[27] The degree of molecular chain orientation value became higher as the D value decreased. This tendency is in agreement with the results of a preceding study.[31] The degree of molecular chain orientation (f_{ch}) of the nanofiber increased from ~0.48 to 0.62, 0.73, and 0.77, at the draw ratio of 1, 3, 4, and 5, respectively (Supporting Information Table S3). Figure 3(e) shows a

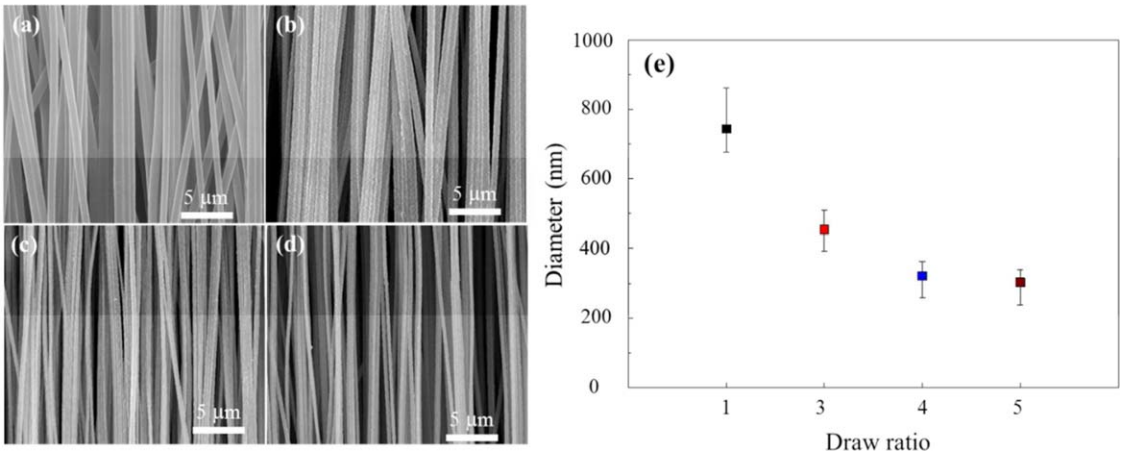

Figure 2. SEM images of aligned and drawn PAN-based nanofiber felts at draw ratio (a) 1 (as-electrospun), (b) 3, (c) 4, and (d) 5. (e) Variation of fiber diameter as a function of stretch ratio. [Color figure can be viewed in the online issue, which is available at wileyonlinelibrary.com.]

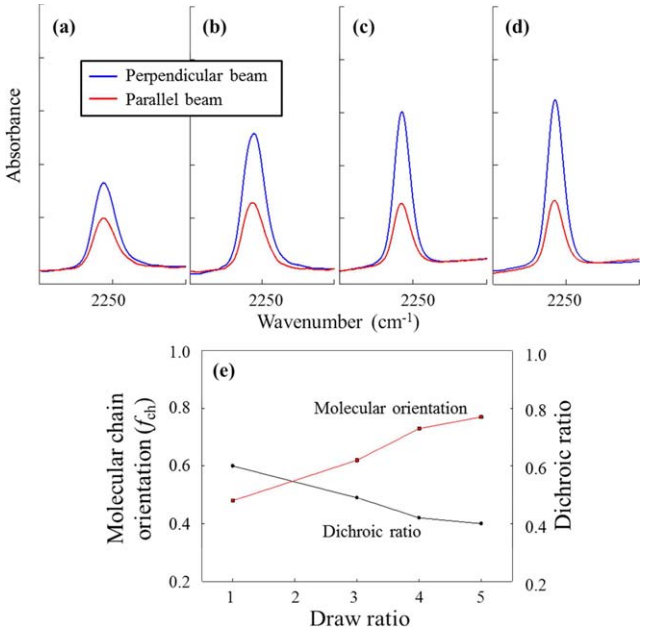

Figure 3. Polarized FT-IR spectra of the PAN nanofibers at draw ratio of (a) 1 (as-electrospun), (b) 3, (c) 4, and (d) 5. (e) The relation of dichroic ratio and the molecular chain orientation with draw ratio. [Color figure can be viewed in the online issue, which is available at wileyonlinelibrary.com.]

similar tendency in the crystallite orientation value (f_{cr}), as shown in Figure 5(b). It indicated that the electrospun PAN nanofibers can achieve a very high degree of molecular chain as well as crystallite orientation through the drawing process, which resulted in enhanced mechanical properties of the nanofiber felts.

The crystallization behavior of the nanofiber felts was investigated by 2D X-ray diffraction analysis [Figure 4(a)]. Sharp diffraction peaks could be observed at a 2θ of around 16.7° and weak diffractions at around 29.0° for all the four samples. These reflections indicated the (100) and (110) planes for the PAN hexagonal lattice.[27] The relative crystallinity and crystallite size gradually increased with an increase in the draw ratio. The full width at half maximum (FWHM) of the two reflection peaks gradually became narrower, whereas the sharpness of the peaks of the drawn nanofibers increased with an increase in the draw ratio. The relative crystallinity for each sample was calculated by the eq. (4).

$$\text{Relative crystallinity} = \frac{\text{Crystalline area}}{\text{Crystalline} + \text{Amorphous area}} \quad (4)$$

The relative crystallinity increased from 40.2 to 60.0% by stretching five times. The crystallite sizes (L_c) of each sample were calculated from the eq. (5), the Scherrer equation.[26,27,38]

$$\text{Crystallite size } (L_c) = \frac{k\lambda}{\beta \cos\theta}\theta \quad (5)$$

where L_c is the crystallite size, θ is the scattering angle, λ is the wavelength of X-ray, β is the width of the diffraction peak measured at half its height (full width at half maximum; FWHM) in radian, and k, the coefficient (pre-factor) of 0.9 was included in the Scherrer's Equation. The average crystallite size also increased by drawing five times, from 37 to 133Å (360% increase), as shown in Figure 4(b). In addition, crystallite orientation degree was calculated by eq. (6).[33,39–42]

$$f_{cr} = \frac{180 - FWHM}{180} \quad (6)$$

where f_{cr} is the orientation factor of the crystallites and FWHM represents the full width at half maximum of the azimuthal profile of (100) peak. The value of f_{cr} became 1 or 0 when the crystallites were aligned perfectly parallel to one another or in random orientation, respectively. Variation of the intensity of (100) reflection peaks for the nanofibers as a function of azimuthal angles is shown in Figure 5(a). Stretching also improved the crystallite orientation from 0.42 (as-electrospun) to 0.58 at the draw ratio 5, which was 138% increase [Figure 5(b)].

On the basis of the above results, it can be concluded that the average crystallinity, crystallite size, and crystallite orientation were improved by stretching the nanofibers, which would promote the crystallization of macromolecules in nanofibers.[28] A high degree of crystallinity and high orientation of the crystalline molecular segments impart high tensile strength and modulus to the fibers,[36] and these experimental results are in good agreement with the polarized FT-IR measurement data.

Thermal behaviors of the electrospun PAN nanofibers and the drawn nanofiber web were characterized by DSC measurements to investigate the influence of drawing (Figure 6). DSC

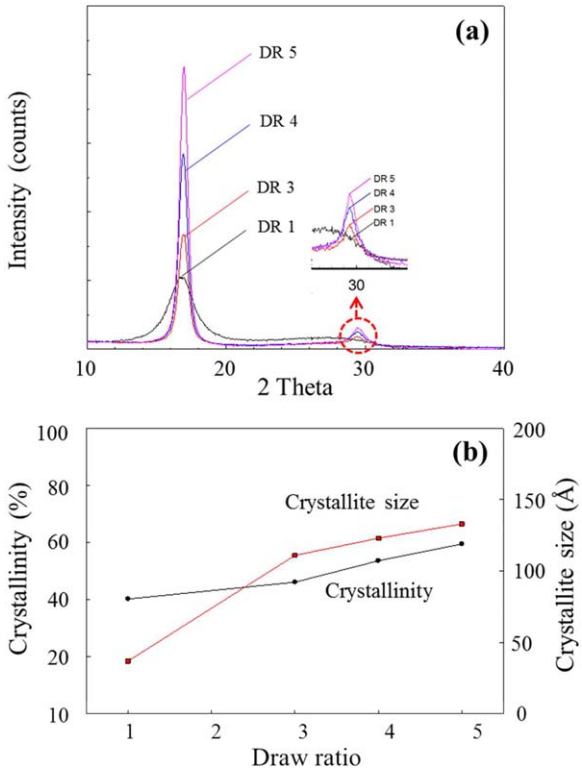

Figure 4. (a) X-ray diffraction pattern of PAN nanofibers for each draw ratio, and (b) the relation of relative crystallinity and crystallite size with draw ratio. [Color figure can be viewed in the online issue, which is available at wileyonlinelibrary.com.]

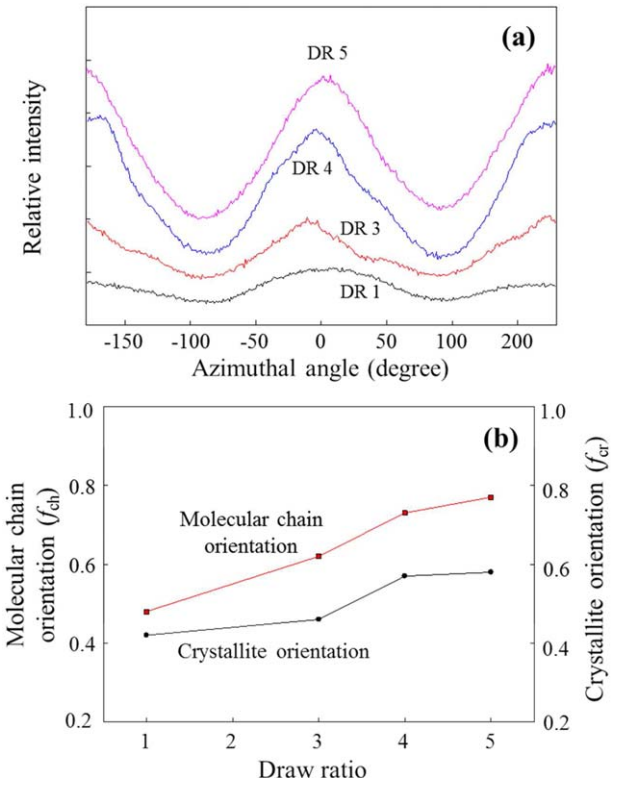

Figure 5. (a) Azimuthal scan of the diffraction pattern at various draw ratio and (b) molecular chain and crystallite orientation as the function of draw ratio. [Color figure can be viewed in the online issue, which is available at wileyonlinelibrary.com.]

measurements were carried out under nitrogen atmosphere. The DSC curves were obtained from the first heating scan because all the curves became flat after a second scan. The T_g of the as-electrospun and the three-times drawn sample were 86.8 °C and 104.5 °C, respectively, whereas no T_g was observed for the four and five-times drawn samples. The clear observation of the T_g at low temperature from the as-electrospun nanofiber, as compared with that of the three times drawn sample can be explained by the entrapped solvent in the nanofibers. Thermal properties of the electrospun PAN nanofibers as a function of draw ratio are summarized in Supporting Information Table S4. The temperature of onsets and exothermic peaks showed the tendency to shift to a lower temperature, while enthalpy changes (ΔH) for the cyclization reaction increased with increase in the draw ratio. The exothermic peaks of the drawn samples became slightly broader than the as-spun samples. It can be inferred that drawing makes the polymer molecules align along the fiber axis and facilitate inter-molecular cyclization of nitrile groups in the PAN macromolecules, as reported in previous studies.[7,23,43,44]

The mechanical properties of PAN-based nanofiber felts were investigated by using the universal testing machine. The cross-sectional area of each specimen was calculated from the weight of each specimen and the density of polyacrylonitrile (1.18 g/cm^3) from the literature.[23,39] The cross-sectional shapes were assumed to be round and 10 samples were tested under each condition. The cross-sectional SEM images of the PAN nanofibers before and after the tensile tests are shown in Supporting Information Figure S7. The samples were fractured in liquid nitrogen. The size of the nanofiber-bundle specimens was 10 mm (width) by 100 mm (length). The thickness of the as-electrospun and drawn PAN nanofiber felts are summarized in Supporting Information Table S5. The representative stress–strain curves of the PAN nanofibers were plotted, as in Figure 7(a). Their mechanical properties such as tensile strength, tensile strain, and tensile modulus are illustrated in Figure 7(b–d) for the as-electrospun, three, four, and five times drawn nanofiber felts, respectively. The values of the tensile strength and strain were averaged from 10 tests. The values of both the tensile strength and modulus of the nanofiber felts increased considerably as the draw ratio increased, indicating powerful effect of aligning and orientation of nanofibers, obtained due to uniaxial molecular chain orientation with improved crystalline properties through uniaxial drawing. The tensile strength of the electrospun PAN-based nanofibers increased from 120 MPa in the as-spun samples to about 630 MPa (improved 525%) in the drawn samples on average and the highest value was around 750 MPa. Additionally, tensile modulus of them increased from 1.5 GPa in the as-spun samples to around 10.6 GPa (improved 667%) in the drawn samples. However, the elongation at break of the felts decreased with increase in the draw ratio. Further research for preventing tensile strain from decreasing due to drawing is thus required. It can be concluded that the electrospun nanofibers were already stretched more than 1,000 times during the electrospinning process due to bending instability and whipping; however, such stretching was still insufficient for maximizing the mechanical properties of PAN nanofibers. The stretching process of the as-spun PAN nanofibers caused much higher degree of molecular chain orientation resulting in the improvement of crystalline properties, structural homogeneity and reducing of defects like voids or beads in the nanofibers. For comparison, commercial PAN fibers (12 K produced by Bluestar Fibers Company Limited) were tested by using UTM

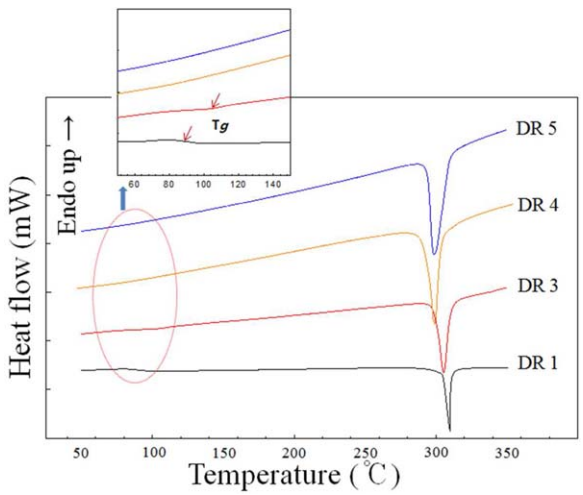

Figure 6. DSC thermograms of electrospun PAN nanofibers as the function of draw ratio. [Color figure can be viewed in the online issue, which is available at wileyonlinelibrary.com.]

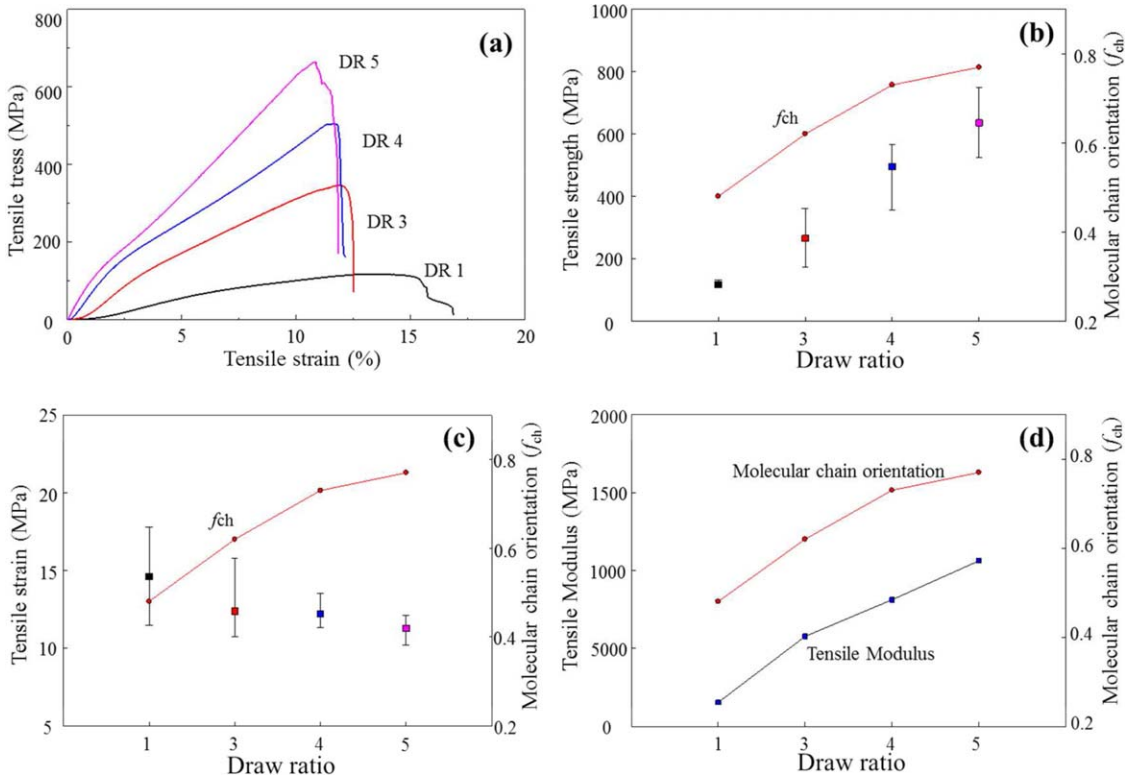

Figure 7. Mechanical properties of PAN nanofiber felts; (a) stress–strain curves, (b) tensile strength, (c) tensile strain, and (d) tensile modulus at various draw ratios. [Color figure can be viewed in the online issue, which is available at wileyonlinelibrary.com.]

(Supporting Information Figure S8). The tensile strength and strain on average of 10 tests were 432 MPa and 28.7%. The tensile modulus was 5,605 MPa. Averaged tensile strength and modulus resulted from this study were higher than those of commercial PAN fiber by 147 and 189%, respectively, while the tensile strain of the commercial samples was much higher than our samples by 254%. The results showed that the electrospun PAN nanofibers, if aligned and drawn optimally, could be an attractive candidate as high-strength nanofibers. Naraghi *et al.*[45,46] evaluated the mechanical properties of electrospun PAN nanofibers with diameters of 300–600 nm using microelectromechanical system. They observed that the tensile strength was in the range from 30 to 130 MPa and the elastic modulus was within 7.6 ± 1.5 GPa. Papkov *et al.*[47] observed the size effect on the mechanical properties of an individual electrospun PAN nanofiber. They reported the largely increased elastic modulus, true strength, and toughness when the diameter of nanofibers is smaller than 250 nm. Interestingly, they observed that the simultaneously increased strength, modulus, and strain at failure led to the drastic increase of toughness. Such an unusual behavior was explained by the fact that the low crystallinity of the electrospun PAN nanofibers due to the rapid solvent evaporation and quick polymer solidification. Even though they used the same polymer (MW 150,000) in dimethylformamide (DMF), however, their solution concentration was low (8–11%) and the distance between the spinneret and collector was long (20 cm) as compared with those of our works. It means that our thick fibers signify slow and incomplete solvent evaporation leading to high crystallization, thereby resulting in the low strain rate at failure. Thus, the judicious combination of low polymer concentration, fine needle, and long distance from needle to collector with high molecular chain orientation could be another solution for achieving high strength fiber with high strain rate. Chen *et al.*[48] also introduced a novel micro tensile testing method to evaluate the mechanical property of an individual electrospun polyimide nanofiber.

Finally, the bulk density of PAN nanofibers was measured from five specimens from each drawing condition (Figure 8). It was increased by 177% when the nanofibers are aligned and drawn. The density of pristine (as-electrospun) samples was 0.19 g/cm^3

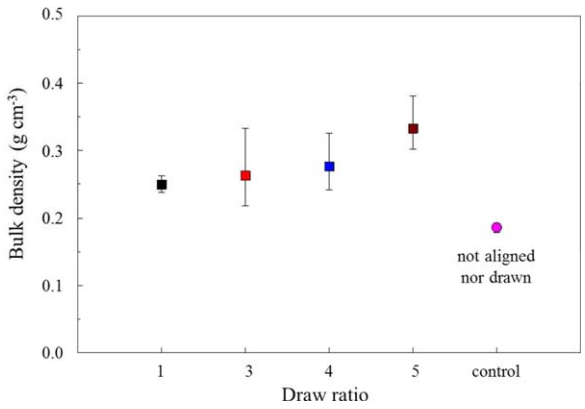

Figure 8. Bulk density of the PAN nanofiber felt as a function of draw ratio. [Color figure can be viewed in the online issue, which is available at wileyonlinelibrary.com.]

on average, which were electrospun at the rotating speed of 100 m/min without deflector plates, whereas the density of the aligned-and-drawn samples was 0.33 g/cm^3 on average at the draw ratio of 5. There was no big increment of bulk density by increasing the draw ratio. It was thus believed that increase in density resulted from a combined effect of nanofiber packing by aligning and crystallite-growing obtained via drawing.[49] Empty spaces were still observed between the nanofibers, as seen in SEM images (Figure 2), which indicated that more close-packing of nanofibers in the electrospun felts is still required to densify them and maximize the fiber performance.

CONCLUSIONS

In this study, attempts have been made to enhance the mechanical properties of PAN-based nanofibers. PAN nanofiber felts with high level of nanofiber-alignment were prepared by electrospinning technique comprising deflector plates and a high speed rotating drum collector during the spinning. A two-step drawing process was followed to improve the crystalline properties and the molecular chain orientation. We achieved additional uniaxial orientation of the molecular chains of PAN nanofibers in the two-step drawing process for largely elongated and aligned nanofibers during electrospinning process. As the draw ratio increased, the tensile properties, crystalline properties (crystallinity, crystallite size), and the molecular chain orientation in the PAN nanofibers were improved, thereby resulting in an enhanced mechanical properties of the PAN-based nanofibers. The tensile strength was increased by 525% via drawing and the highest value was around 750 MPa. Tensile modulus and the bulk density were increased by 667% and 177%, respectively by aligning and drawing. This, it can be concluded that optimization of both aligning and drawing processes are critical to obtain high-performance PAN-based nanofibers.

ACKNOWLEDGMENTS

Y.A.K acknowledges the financial support from the National Research Foundation of Korea (NRF) grant funded by the Korea government (MSIP) (No. NRF-2014R1A2A1A10050585) and from the framework of international cooperation program managed by the National Research Foundation of Korea (NRF-2015K2A2A4000110, FY2015).

REFERENCES

1. Gu, S. Y.; Wu, Q. L.; Jie, R. *New Carbon Mater.* **2008**, *23*, 171. [TQ1]
2. Kim, Y. A.; Hayashi, T.; Endo, M.; Dresselhaus, M. S. Carbon Nanofiber. In Springer Handbook of Nanomaterials; Vajtai, R., Ed.; Springer: Berlin/Heidelberg, Germany, **2013**; pp 233–262.
3. Zussman, E.; Chen, X.; Ding, W.; Calabri, L.; Dikin, D.; Quintana, J.; Ruoff, R. *Carbon* **2005**, *43*, 2175.
4. Sautter, B. Department of Mechanical Engineering, University of Illinois, Chicago, **2005**.
5. Xu, F.; Beyazoglu, T.; Hefner, E.; Gurkan, U. A.; Demirci, U. *Tissue Eng. C Meth.* **2011**, *17*, 641.
6. Yao, J.; Bastiaansen, C. W.; Peijs, T. *Fibers* **2014**, *2*, 158.
7. Gu, S.; Ren, J.; Wu, Q. *Synth. Met.* **2005**, *155*, 157.
8. Huang, Z. M.; Zhang, Y. Z.; Kotaki, M.; Ramakrishna, S. *Compos. Sci. Technol.* **2003**, *63*, 2223.
9. Yang, Y.; Simeon, F.; Hatton, T. A.; Rutledge, G. C. *J. Appl. Polym. Sci.* **2012**, *124*, 3861.
10. Arras, M. M.; Grasl, C.; Bergmeister, H.; Schima, H. *Sci. Technol. Adv. Mater.* **2012**, *13*, 035008.
11. Greiner, A.; Wendorff, J. H. *Angew. Chem.* **2007**, *46*, 5670.
12. Koski, A.; Yim, K.; Shivkumar, S. *Mater. Lett.* **2004**, *58*, 493.
13. Wang, C.; Hsu, C. H.; Lin, J. H. *Macromolecules* **2006**, *39*, 7455.
14. Fong, H.; Chun, I.; Reneker, D. H. *Polymer* **1999**, *40*, 4585.
15. Sadrjahani, M.; Hoseini, S.; Mottaghitalab, V.; Haghi, A. *Braz. J. Chem. Eng.* **2010**, *27*, 583.
16. Song, Z.; Hou, X.; Zhang, L.; Wu, S. *Materials* **2011**, *4*, 621.
17. Xie, Z.; Niu, H.; Lin, T. *RSC Adv.* **2015**, *5*, 15147.
18. Kiselev, P.; Rosell-Llompart, J. *J. Appl. Polym. Sci.* **2012**, *125*, 2433.
19. Richard-Lacroix, M.; Pellerin, C. *Macromolecules* **2013**, *46*, 9473.
20. Zhang, C.; Ding, X.; Wu, S. *Nanofibers* **2011**, *458*,
21. Fennessey, S. F.; Farris, R. J. *Polymer* **2004**, *45*, 4217.
22. Liao, C. C.; Wang, C. C.; Chen, C. Y.; Lai, W. J. *Polymer* **2011**, *52*, 2263.
23. Liu, J.; Chen, G.; Gao, H.; Zhang, L.; Ma, S.; Liang, J.; Fong, H. *Carbon* **2012**, *50*, 1262.
24. Liu, Y.; Zhang, X.; Xia, Y.; Yang, H. *Adv. Mater.* **2010**, *22*, 2454.
25. Li, D.; Wang, Y.; Younan, X. *Adv. Mater* **2004**, *16*, 361.
26. Zhou, Z.; Lai, C.; Zhang, L.; Qian, Y.; Hou, H.; Reneker, D. H.; Fong, H. *Polymer* **2009**, *50*, 2999.
27. Lai, C.; Zhong, G.; Yue, Z.; Chen, G.; Zhang, L.; Vakili, A.; Wang, Y.; Zhu, L.; Liu, J.; Fong, H. *Polymer* **2011**, *52*, 519.
28. Liu, J.; Liu, Q.; Ma, S.; Liang, J.; Ma, X.; Fong, H. *Polymer* **2013**, *54*, 4987.
29. Yu, D. G.; Chou, W. L.; Yang, M. C. *Sep. Purif. Technol.* **2006**, *52*, 380.
30. Wangxi, Z.; Jie, L.; Gang, W. *Carbon* **2003**, *41*, 2805.
31. Liu, J.; He, L.; Ma, S.; Liang, J.; Zhao, Y.; Fong, H. *Polymer* **2015**, *61*, 20.
32. Li, X.; Liu, C. Y.; Qin, A. W.; Zhao, X. Z.; Ma, B. M.; He, C. J. *Mater. Sci. Forum* **2014**, 617. pp
33. Tao, D.; Higaki, Y.; Ma, W.; Wu, H.; Shinohara, T.; Yano, T.; Takahara, A. *Polymer* **2015**, *60*, 284.
34. Kongkhlang, T.; Tashiro, K.; Kotaki, M.; Chirachanchai, S. *J. Am. Chem. Soc.* **2008**, *130*, 15460.
35. Yano, T.; Higaki, Y.; Tao, D.; Murakami, D.; Kobayashi, M.; Ohta, N.; Koike, J.; Horigome, M.; Masunaga, H.; Ogawa, H. *Polymer* **2012**, *53*, 4702.
36. Davidson, J.; Jung, H. T.; Hudson, S.; Percec, S. *Polymer* **2000**, *41*, 3357.

37. Bashir, Z.; Tipping, A. R.; Church, S. P. *Polym. Int.* **1994**, *33*, 9.

38. Mathur, R.; Bahl, O.; Kundra, K. *J. Mater. Sci. Lett.* **1986**, *5*, 757.

39. Tsai, J. S. *J. Mater. Sci. Lett.* **1992**, *11*, 140.

40. Kim, I. M.; Yoo, M. K.; Kim, K. J. *Text. Sci. Eng.* **2013**, *50*, 25.

41. Son, K. S.; Gu, J. G.; Yoon, W. S.; Chang, D. H. *Text. Color. Finish.* **1996**, *8*, 33.

42. Bang, Y. H.; Lee, C. Y.; Kim, H. D.; Lee, M. C.; Cho, H. H. *Text. Color. Finish.* **1995**, *7*, 24.

43. Jung, K.; Hwang, D.; Shul, Y.; Han, H.; Lee, W. *Mater. Lett.* **2002**, *53*, 180.

44. Hou, X.; Yang, X.; Zhang, L.; Waclawik, E.; Wu, S. *Mater. Des.* **2010**, *31*, 1726.

45. Naraghi, M.; Chasiotis, I.; Kahn, H.; Wen, Y. K.; Dzenis, Y. A. *Appl. Phys. Lett.* **2007**, *91*, 151901.

46. Naraghi, M.; Chasiotis, I.; Kahn, H.; Wen, Y. K.; Dzenis, Y. A. *Rev. Sci. Instrum.* **2007**, *78*, 085108.

47. Papkov, D.; Zou, Y.; Andalib, M. N.; Goponenko, A.; Cheng, S. Z. D.; Dzenis, Y. A. *ACS Nano* **2013**, *7*, 3324.

48. Chen, F.; Peng, X.; Li, T.; Chen, S.; Wu, X. F.; Reneker, D. H.; Hou, H. *J. Phys. D Appl. Phys.* **2008**, *41*, 025308.

49. Huang, X. *Materials* **2009**, *2*, 2369.